Eur. Phys. J. E (2016) **39**: 43
DOI 10.1140/epje/i2016-16043-4

THE EUROPEAN PHYSICAL JOURNAL E

Regular Article

Confinement effects on the miscibility of block copolymer blends

Russell K.W. Spencer[a] and Mark W. Matsen[b]

Department of Chemical Engineering, Department of Physics & Astronomy, and the Waterloo Institute for Nanotechnology, University of Waterloo, Waterloo, Ontario, Canada

Received 21 February 2016 and Received in final form 26 March 2016
Published online: 22 April 2016 –

Abstract. Thin films of long and short symmetric AB diblock copolymers are examined using self-consistent field theory (SCFT). We focus on hard confining walls with a preference for the A component, such that the lamellar domains orient parallel to the film with an even number ν of monolayers. For neat melts, confinement causes the lamellar period, D, to deviate from its bulk value, D_b, in order to be commensurate with the film thickness, *i.e.*, $L = \nu D/2$. For blends, however, the melt also has the option of macrophase separating into $\nu^{(\ell)}$ large and $\nu^{(s)}$ small monolayers so as to provide a better fit, where $L = \nu^{(\ell)}D^{(\ell)}/2 + \nu^{(s)}D^{(s)}/2$. In addition to performing full SCFT calculations of the entire film, we develop a semi-analytical calculation for the coexistence of thick and thin monolayers that helps explain the complicated interplay between miscibility and commensurability.

1 Introduction

Confinement of block copolymer melts can have a dramatic impact on their behavior, because of the need for their domains to conform to the confining space. Initial theoretical calculations [1] and experiments [2,3] on confinement effects focused on symmetric AB diblock copolymers sandwiched between two hard walls separated by a distance L. Not only are thin films a good system for studying the fundamentals of block copolymer phase behavior [3–8], they also possess useful applications including nanolithography, surface patterning, porous membranes, reflective surfaces and nanoelectronics [9–15]. In the last few years, interest has mushroomed with the development of new confinement geometries (*e.g.*, cylindrical pores and spherical cavities) further extending the range of applications [16,17]. In efforts to gain greater control and to access a wider diversity of microstructures, researchers have begun to investigate more complicated block copolymer architectures as well as blends [18–28]. Blending is the simpler way of controlling morphology, especially compared to synthesizing new block copolymers, but blends are also prone to immiscibility issues [18–22].

To illustrate the convenience of blending, consider mixtures large and small versions of the same block copolymer with N_ℓ and N_s degrees of polymerization, respectively. By simply adjusting the volume fraction of short diblock, $\bar{\phi}_s$, one can vary the preferred period, D_b, from that of the large molecule to that of the small molecule [29]. Naturally, the more the size ratio $\alpha \equiv N_s/N_\ell$ deviates from one, the greater the range over which the period can be adjusted. However, it is known that blends of large and small diblocks will macrophase separate in the bulk if α differs too much from one [30–32]. Furthermore, the frustration due to confinement may exacerbate the immiscibility.

The simplest and most natural system for studying confinement effects on blends is a thin film of long and short lamellar-forming diblock copolymers. Indeed, there have already been several experiments [4,18,19] on this system, but they have only scratched the surface. Despite its relative simplicity, the parameter space for this system is still rather large. From a theoretical perspective, the natural starting point is that of blends confined between parallel walls with a surface affinity that causes the lamellar microstructure to orient parallel to the film with ν monolayers between the two walls. If both surfaces favor the same component (*i.e.*, symmetric wetting) then ν takes on an even integer, whereas it is odd for asymmetric wetting. In cases where one of the two surfaces is relatively neutral, all integer values of ν are allowed. If the two diblock copolymers mix, then the melt adopts a single lamellar period $D = 2L/\nu$, where ν is selected so as to best approximate the bulk period D_b (see fig. 1a). However, if the blend macrophase separates then it has two lamellar periods with which to find a better fit to the confining geometry. The macrophase separation can occur in the normal or lateral directions as illustrated in figs. 1b and c, respectively. The former should happen relatively quickly as it only requires a local rearrangement of molecules, while the latter is likely beyond accessible time scales as it requires the macroscopic transport of material; we will have more to say about this later.

[a] e-mail: r6spence@uwaterloo.ca
[b] e-mail: mwmatsen@uwaterloo.ca

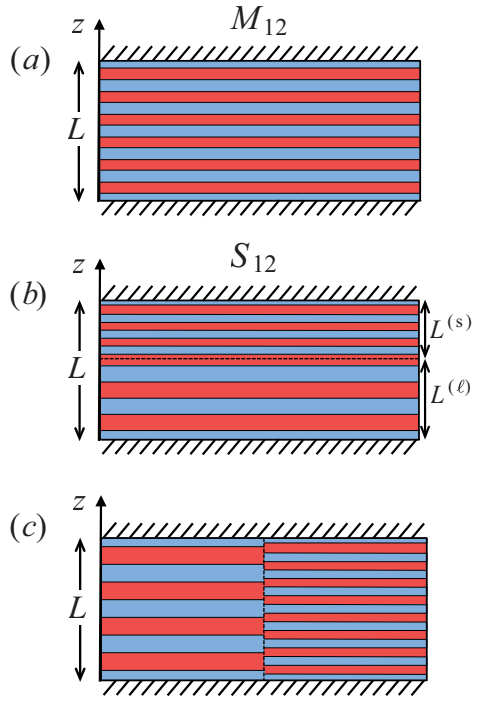

Fig. 1. Schematic diagrams of lamellar morphologies in confined films of long and short symmetric diblock copolymers, illustrating (a) uniform mixing, (b) macrophase separation normal to the film and (c) macrophase separation in the lateral direction. The morphologies in (a) and (b) are denoted by M_ν and S_ν, respectively, where $\nu = 12$ refers to the number of monolayers.

In this initial study, we construct phase diagrams showing the tendency for macrophase separation normal to the film. This is done by comparing the free energies of the M_ν and S_ν morphologies in fig. 1, using self-consistent field theory (SCFT). In addition to the full SCFT calculation, we also devise a simple semi-analytical calculation that helps illustrate the complicated interplay of issues that determine the preferred morphology.

2 Theory

The specific system of this study is an incompressible blend of n_ℓ large AB diblock copolymers each with N_ℓ segments and n_s small AB diblock copolymers with N_s segments, confined between two flat parallel walls separated by a distance L. The polymerization of the large polymer is use as our reference and the relative size of the small polymer is specified by $\alpha \equiv N_s/N_\ell$. For convenience, the A and B segments are defined based on a common volume, ρ_0^{-1}, such that the total volume of the film is $V = (n_\ell N_\ell + n_s N_s)/\rho_0$ and the volume fraction of small molecules (*i.e.*, the composition of the blend) is $\bar{\phi}_s = n_s N_s/\rho_0 V$. The incompatibility between unlike segments that drives microphase separation is controlled by the usual Flory-Huggins parameter, χ. The present study is restricted to perfectly symmetric diblock copolymers with equal numbers of A and B segments of the same statistical length a, for which the simple lamellar phase is preferred.

The statistical mechanics of this system are solved using self-consistent field theory (SCFT), where the molecular interactions experienced by a γ-type segment (γ = A or B) are represented by the field $w_\gamma(z)$. Since we are restricting our attention to layered morphologies that are uniform in the lateral direction, the fields will only depend on the z coordinate normal to the film. The first step of SCFT is to evaluate propagators or partial partition functions by solving diffusion equations, for which we use a fourth-order pseudo-spectral method [33,34]. The two surfaces at $z = 0$ and $z = L$ are treated by invoking reflecting boundary conditions [35]. From the propagators, we can immediately calculate the single-chain partition function, Q_δ, and the γ-type segment concentration, $\phi_{\delta,\gamma}(z)$, of the δ-sized molecules ($\delta = \ell$ or s). Once we have the concentrations, the fields are adjusted using Anderson mixing [34] until they satisfy

$$w_A(z) = \chi N_\ell \phi_B(z) + \xi(z) \ , \tag{1}$$

$$w_B(z) = \chi N_\ell \phi_A(z) + \xi(z) \ , \tag{2}$$

where $\phi_\gamma(z) \equiv \phi_{\ell,\gamma}(z) + \phi_{s,\gamma}(z)$ is the total concentration of γ-type segments and $\xi(z)$ is the pressure field that enforces incompressibility, $\phi_{\rm A}(z)+\phi_{\rm B}(z) = 1$. The field equations generally exhibit a number of distinct self-consistent solutions (or morphologies). The relative stability of a morphology is determined by evaluating its canonical free energy,

$$\frac{F_c N_\ell}{k_B T \rho_0 V} = (1-\bar{\phi}_s)\ln\left(\frac{1-\bar{\phi}_s}{Q_\ell}\right) + \frac{\bar{\phi}_s}{\alpha}\ln\left(\frac{\bar{\phi}_s}{Q_s}\right) + \frac{1}{L}\int [\chi N_\ell \phi_{\rm A}(z)\phi_{\rm B}(z) - w_{\rm A}(z)\phi_{\rm A}(z) - w_{\rm B}(z)\phi_{\rm B}(z)]{\rm d}z \ . \tag{3}$$

Note that our derivation does not explicitly include the surface affinity of the walls that generally appears in the theory [36]. We will be dealing with melts that are highly segregated, such that the surface interactions have a negligible effect on the level of segregation. All they do is basically exclude the morphologies with an unfavorable component next to either wall. We can do this ourselves by restricting the candidate morphologies appropriately.

By using reflecting boundary conditions without explicitly including surface interactions, the above SCFT calculation can be applied as is to bulk blends. For the bulk system, one simply sets the system size to half a lamellar period (*i.e.*, $L = D_b/2$) corresponding to a single monolayer extending between the centers of two neighboring A and B domains. Naturally, the free energy, F_c, has to be minimized with respect to the bulk period, D_b. The only difference for the film calculation is that L is fixed at a relatively large value, such that the system contains a number, ν, of monolayers.

The self-consistent solution for the mixed M_ν morphology with ν identical monolayers (see fig. 1a) is easily

found, but the solution for the macrophase-separated S_ν morphology with a phase of $\nu^{(s)}$ small monolayers coexisting with a phase of $\nu^{(\ell)}$ large monolayers (see fig. 1b) can be challenging to locate. For this, we develop a simple semi-analytical calculation, where we assume the film thickness,

$$L = L^{(\ell)} + L^{(s)} \ , \tag{4}$$

separates into two lamellar phases with periods $D^{(\delta)} = 2L^{(\delta)}/\nu^{(\delta)}$ and compositions $\bar{\phi}_s^{(\delta)}$ ($\delta = \ell$ or s). Naturally, the conservation of small diblock copolymer implies that

$$L\bar{\phi}_s = L^{(\ell)}\bar{\phi}_s^{(\ell)} + L^{(s)}\bar{\phi}_s^{(s)} \ . \tag{5}$$

The canonical free energy density, $f_c \equiv F_c/V$, of the S_ν morphology is given by

$$Lf_c = L^{(\ell)}f_c^{(\ell)} + L^{(s)}f_c^{(s)} + \Gamma_b \ , \tag{6}$$

where $f_c^{(\delta)}$ is the free energy density of the δ phase and Γ_b is the boundary tension between the two phases. The equilibrium is found by minimizing f_c with respect to the size $L^{(\delta)}$ and composition $\bar{\phi}_s^{(\delta)}$ of each phase, subject to the constraints in eqs. (4) and (5). This results in the two conditions:

$$\mu^{(\ell)} = \mu^{(s)} \ , \tag{7}$$

$$f_g^{(\ell)} = f_g^{(s)} \ , \tag{8}$$

where

$$\mu \equiv \frac{\partial f_c}{\partial \bar{\phi}_s} \tag{9}$$

is a chemical potential and

$$f_g \equiv f_c + \frac{\partial f_c}{\partial D}D - \mu\bar{\phi}_s \tag{10}$$

is a generalized free energy density.

Although the semi-analytical calculation needs to adjust $L^{(\delta)}$ and $\bar{\phi}_s^{(\delta)}$ for each phase, it is still generally much faster than the full SCFT calculation particularly for thick films, because it only needs to solve for a single monolayer from each phase. There is also the advantage that the convergence to a self-consistent solution is more stable. Admittedly, the semi-analytical procedure does require the boundary tension, Γ_b, but it only needs to be evaluated once for each blend (*i.e.*, each combination of χN_ℓ and α) [37][1].

3 Results

The parameter space of our system is too large to study completely, and so we focus on blends with $\chi N_\ell = 200$ and $\alpha = 0.1$, in which case even the short diblock copolymer has a high segregation strength of $\chi N_s = 20$. This ensures that the A and B components remain well segregated, which is the requirement allowing us to account for the surface affinity implicitly by just considering candidate morphologies with the appropriate component next to each wall.

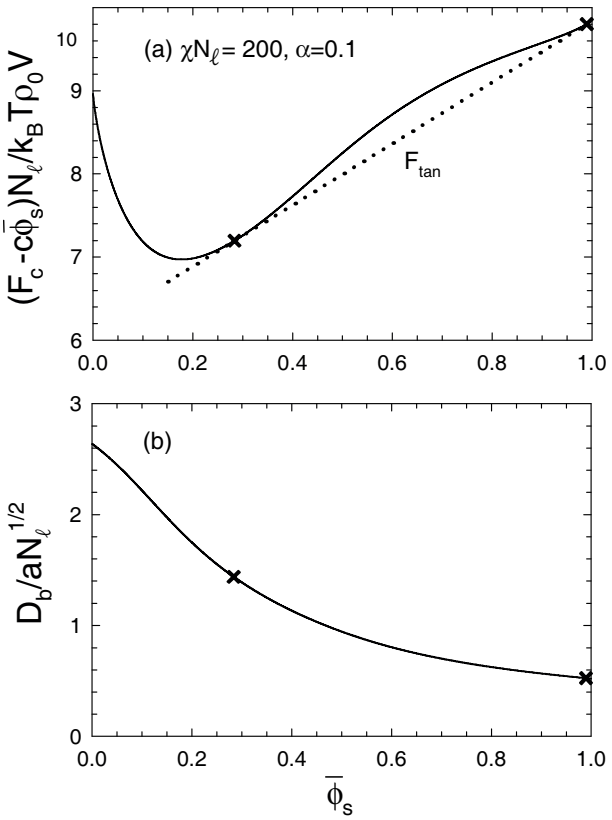

Fig. 2. (a) Canonical free energy, F_c, and (b) period, D_b, of the bulk lamellar phase plotted as functions of blend composition, $\bar{\phi}_s$, for $\chi N_\ell = 200$ and $\alpha = 0.1$. For clarity, the slope of F_c has been reduced by some constant, c. The double-tangent line, $F_{\tan}$, in plot (a) determines the compositions, $\bar{\phi}_s^{(\ell)} = 0.2836$ and $\bar{\phi}_s^{(s)} = 0.9895$, and periods, $D_b^{(\ell)} = 1.442aN_\ell^{1/2}$ and $D_b^{(s)} = 0.526aN_\ell^{1/2}$, of coexisting lamellar phases.

Before examining the thin films, it is useful to establish the bulk phase behavior. The free energy of a bulk blend is plotted in fig. 2 as a function of its composition, $\bar{\phi}_s$. The double-tangent construction conveniently determines the two-phase region, $0.2836 < \bar{\phi}_s < 0.9895$, and provides the periods of the coexisting lamellar phases. This gives us an idea of what to expect for thin film blends.

Turning now to thin films, we begin by considering blends of compositions $\bar{\phi}_s = 0.38$ and 0.5, confined between walls with an affinity for the A component and a separation of $L = 3.2aN_\ell^{1/2}$. Based on the bulk behavior, we could expect the film to macrophase separate. The number of large and small monolayers can be estimated from the bulk behavior in fig. 2 by using the lever rule,

$$\frac{\nu^{(s)}}{\nu^{(\ell)}} = \frac{D_b^{(\ell)}(\bar{\phi}_s - \bar{\phi}_s^{(\ell)})}{D_b^{(s)}(\bar{\phi}_s^{(s)} - \bar{\phi}_s)} \ , \tag{11}$$

[1] The boundary tension for the parameters of our blend is $\Gamma_b = 0.2836k_BTa\rho_0N_\ell^{-1/2}$.

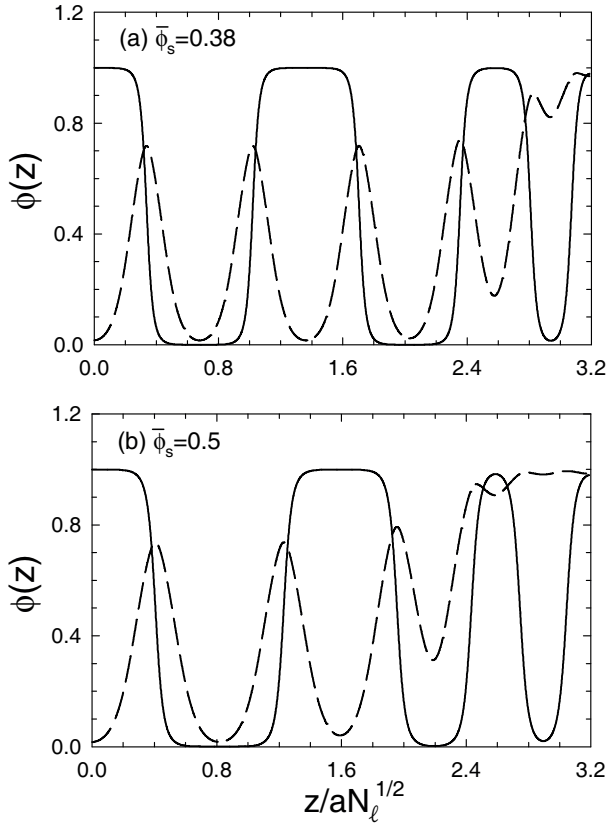

Fig. 3. A-segment concentration, $\phi_A(z)$, (solid curves) and short-polymer concentration, $\phi_s(z)$, (dashed curves) in the S_6 morphology, calculated for films of thickness $L = 3.2aN_\ell^{1/2}$ and compositions (a) $\bar{\phi}_s = 0.38$ and (b) $\bar{\phi}_s = 0.5$.

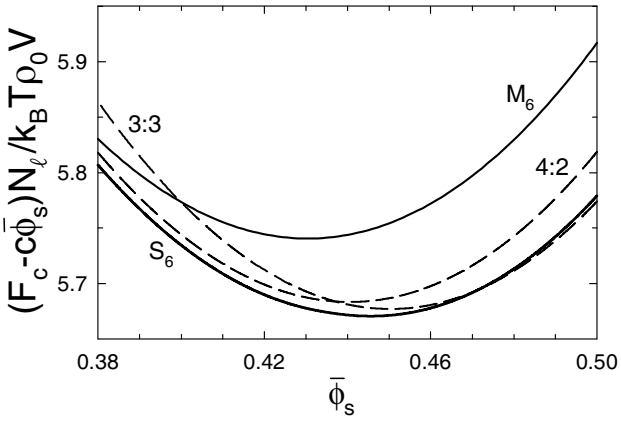

Fig. 4. Free energy, F_c, of the mixed M_6 and macrophase-separated S_6 morphologies. Semi-analytical approximations for S_6 with $\nu^{(\ell)}$:$\nu^{(s)}$ = 4:2 and 3:3 are plotted with dashed curves. For clarity, the slopes of the free energy curves have been reduced by a constant, c.

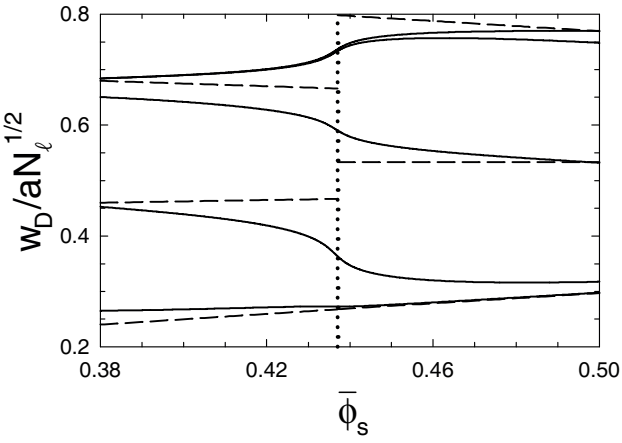

Fig. 5. Widths, w_D, of the five inner domains of the S_6 phase in fig. 3 plotted as a function of composition, $\bar{\phi}_s$. The full and semi-analytical predictions are shown with solid and dashed curves, respectively. The latter predicts a discontinuous transition from $\nu^{(\ell)}$:$\nu^{(s)}$ = 4:2 on the left of the dotted line to 3:3 on the right.

in conjunction with $L = \nu^{(\ell)}D_b^{(\ell)}/2 + \nu^{(s)}D_b^{(s)}/2$. Solving these equations gives $\nu^{(\ell)}$:$\nu^{(s)}$ = 3.83:1.66 and 3:08:3.73 for $\bar{\phi}_s$ = 0.38 and 0.5, respectively. Given that $\nu^{(\ell)}$ and $\nu^{(s)}$ must be integers adding up to an even number (*i.e.*, symmetric wetting), we should expect macrophase separation with $\nu^{(\ell)}$:$\nu^{(s)}$ = 4:2 and 3:3, respectively. Indeed, the self-consistent solutions from the full SCFT, shown in fig. 3, correspond to the S_6 morphology with these particular ratios of large and small monolayers. Note that the total number of monolayers, $\nu = \nu^{(\ell)} + \nu^{(s)}$, is readily determined by counting the A/B interfaces, defined by $\phi_A(z) = 0.5$. We can also see that the large and small lamellae are reasonably consistent with the compositions $\bar{\phi}_s^{(\delta)}$ and periods $D_b^{(\delta)}$ predicted for the bulk behavior in fig. 2.

The stability of the macrophase-separated S_6 morphology relative to the mixed M_6 one partly depends on how well it fits the film thickness L. For instance, the 4:2 configuration at $\bar{\phi}_s = 0.38$ prefers a thickness of about $2D_b^{(\ell)} + D_b^{(s)} = 3.41aN_\ell^{1/2}$ which is a superior match to L than the preferred thickness $3D_b = 3.53aN_\ell^{1/2}$ of the M_6 morphology. However, there are other issues to consider such as the free energy cost per unit area, Γ_b, of forming a boundary between large and small lamellae as well as the natural preference for macrophase separation. To determine which morphology is favored requires calculation of the free energies, shown in fig. 4. As it turns out, S_6 is indeed more stable than M_6.

Figure 4 also includes the semi-analytical predictions for $\nu^{(\ell)}$:$\nu^{(s)}$ = 4:2 and 3:3 corresponding to the morphologies in figs. 3a and 3b, respectively. As expected, the first curve is accurate at small $\bar{\phi}_s$, while the second is accurate at large $\bar{\phi}_s$. However, there is one significant different between the full SCFT calculation and the semi-analytical calculation. The former predicts a smooth free energy implying that the morphology in fig. 3a evolves continuously into that of fig. 3b as $\bar{\phi}_s$ increases, whereas the semi-analytical calculation predicts a discontinuous phase transition from $\nu^{(\ell)}$:$\nu^{(s)}$ = 4:2 to 3:3 at $\bar{\phi}_s = 0.437$.

To understand the difference between the full and semi-analytical calculations, fig. 5 plots the widths, w_D,

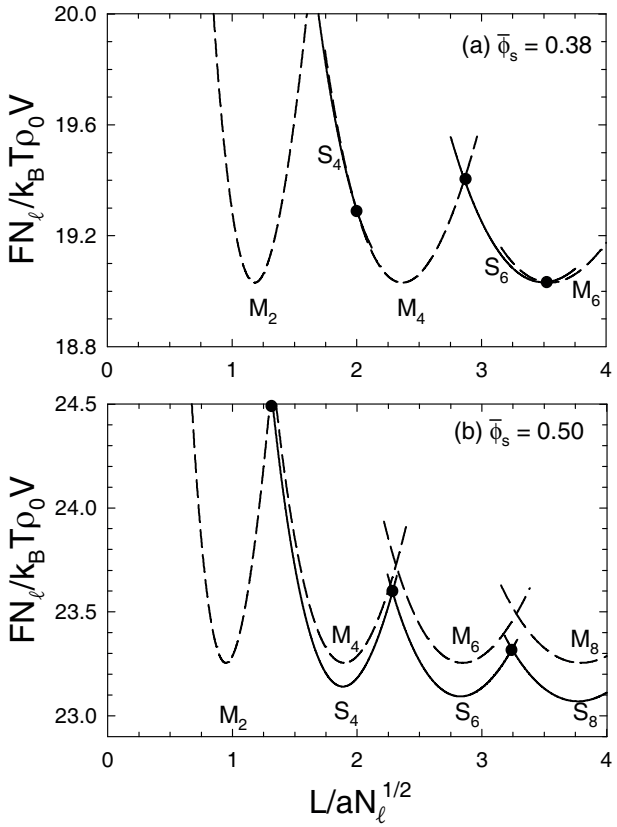

Fig. 6. Free energies, F_c, of macrophase-separated S_ν (solid curves) and mixed M_ν (dashed curves) morphologies calculated for (a) $\bar{\phi}_s = 0.38$ and (b) $\bar{\phi}_s = 0.5$, using the full SCFT. The solid dots denote phase transitions.

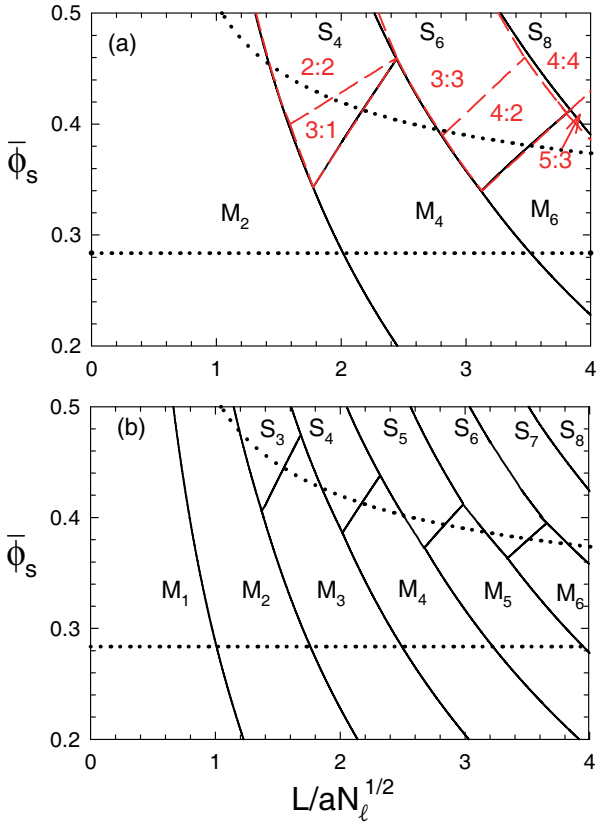

Fig. 7. Phase diagrams for confined films with (a) symmetric wetting and (b) one neutral wall. The top diagram shows the different $\nu^{(\ell)}$:$\nu^{(s)}$ combinations predicted by the semi-analytical calculation. The horizontal dotted lines show the binodal, $\bar{\phi}_s = 0.2836$, beyond which bulk melts macrophase separate, while the dotted curves shows the approximate binodal for thin films obtained by including the boundary tension, Γ_b, between the coexisting large and small lamellae.

of the five inner domains of S_6 (defined by $\phi_A(z) = 0.5$) as a function of $\bar{\phi}_s$. We would have plotted the widths of the monolayers, except that they are not well-defined in the full calculation. In the semi-analytical calculation, there are $\nu^{(\ell)} - 1$ large domains of width $D^{(\ell)}/2$, $\nu^{(s)} - 1$ small domains of width $D^{(s)}/2$ and one intermediate domain of width $(D^{(\ell)} + D^{(s)})/4$ at the boundary. As we can see, there is discontinuous change in the widths at the phase transition identified in fig. 4. In contrast, the full SCFT calculation shows a continuous variation in the widths. As $\bar{\phi}_s$ increases from 0.38 to 0.50, the intermediately sized domain at the boundary becomes small, while one of the large domains adopts the intermediate width. Although the transformation is technically continuous, there is a fairly abrupt crossover that coincides with the transition predicted by the semi-analytical calculation. Indeed, we find that the erroneous transitions ($\nu^{(\ell)} \to \nu^{(\ell)} \pm 1$ and $\nu^{(s)} \to \nu^{(s)} \mp 1$) predicted by the semi-analytical calculation do correspond to abrupt changes in the morphology. Although we see no clear indication of it for the thin films of our study, these abrupt crossovers predicted by the full SCFT would undoubtedly become sharper eventually turning into discontinuous transitions for sufficiently thick films.

To construct phase diagrams, we need to compare the free energies of all the potential morphologies. Figure 6 shows the comparison as a function of film thickness at two different compositions, calculated using the full SCFT. In this case, we only consider even values of ν, corresponding to symmetric wetting, where an A-rich domain resides next to each wall. Of course, the morphology with the lowest free energy is the stable one, and thus the phase transitions occur at the crossings denoted by solid dots. The semi-analytical calculation is much the same, except that for each macrophase-separated S_ν morphology we need to consider different combinations of large and small monolayers with $\nu = \nu^{(\ell)} + \nu^{(s)}$.

Figure 7 shows the resulting phase diagram for thin films, mapping the stability regions of the various M_ν and S_ν morphologies over the parameter space, L and $\bar{\phi}_s$. The top plot corresponds to symmetric wetting where ν is restricted to even values, while the lower plot corresponds to films with one neutral wall for which all integer values are allowed. In the first case, we also plot the phase boundaries from the semi-analytical calculation (dashed curves). The agreement with the full calculation is excellent. The only

difference is that the semi-analytical calculation predicts addition phase transitions in the S_ν regions for different combinations of $\nu = \nu^{(\ell)} + \nu^{(s)}$. However, as we have already demonstrated, these erroneous transitions do correspond with abrupt changes in the full calculation, and so they are in fact meaningful. They are omitted from fig. 7b, just because the diagram is already quite crowded.

4 Discussion

As mentioned in the Introduction, we ignore the possibility of macrophase separation in the lateral direction (see fig. 1c). The free energy of the resulting morphologies would be straightforward to calculate, and would undoubtedly represent the global minimum in certain regions of the phase diagrams in fig. 7. However, we expect that these morphologies are kinetically inaccessible for normal experimental conditions [20, 22], where the film is created by spin-coating the blend onto a substrate producing a laterally uniform composition. From this initial state, macrophase separation in the normal direction should be reasonably facile given that it only requires a short-range exchange of molecules between the top and bottom of the film. On the other hand, macrophase separation in the lateral direction would require the exchange of material over much larger distances. To realize an actual reduction in free energy would entail nucleating regions of the coexisting phases large enough that the free energy gain of macrophase separation compensates for the boundary tension between the phases. The fact that the free energy gain is tiny (see fig. 2) and the boundary tension of large and small lamellae joining up end-to-end would be considerable (see fig. 1c) implies that the critical nucleus size would be enormous. As such, macrophase separation is unlikely to occur laterally over any realistic timescale.

Experiments by Zhang *et al.* [18] support our assertion that macrophase separation is restricted to the normal direction. They considered a blend with $\alpha \approx 0.13$, close to the value we examined, but their surfaces were relatively neutral, although not perfectly so. Interestingly, neat films of their large diblock formed perpendicular lamellae, while those of the small diblock formed parallel lamellae. Consequently, when their thin-film blends underwent macrophase separation, the coexisting phases adopted different orientations. Nevertheless, the separation only occurred in the normal direction despite the fact that the boundary tension, Γ_b, between perpendicular lamellae would be much higher than between the parallel lamellae of our study. Thus we can be confident that macrophase separation in the lateral direction is also kinetically inaccessible for the conditions of our study.

The principle aim of our study was to investigate the impact of confinement on macrophase separation. The first important observation from our phase diagrams is that the region of macrophase separation in thin films is reduced from that of the bulk phase, $0.2836 < \bar{\phi}_s < 0.9895$; the lower binodal of this interval is denoted in fig. 7 by horizontal dotted lines. The reduction can be attributed to the unfavorable boundary tension, which effectively raises the double-tangent line, $F_{\tan}$, in fig. 2 by $V\Gamma_b/L$. The dotted curve in fig. 7 shows the resulting shift in the binodal, which indeed passes though the middle of the sawtooth boundary between the mixed M_ν and phase-separated S_ν morphologies. Our semi-analytical calculation provides the simple explanation for the sawtooth deviations from the dotted curve. Macrophase separation is enhanced when the preferred thickness, $\nu^{(\ell)}D_b^{(\ell)}/2 + \nu^{(s)}D_b^{(s)}/2$, of the S_ν morphology provides a better match to the film thickness, L, than the preferred thickness, $\nu D_b/2$, of the M_ν morphology, and vice versa. As it happens, this confinement-induced effect is smaller than the shift due to Γ_b. This is because Γ_b is reasonable large; in fact it is approximately 5% the size of the A/B interfacial tension[2]. This will be good news for those wanting to use blending to tune the behavior of a block copolymer morphology (*e.g.*, its preferred domain size), for which immiscibility would be an unwelcome occurrence.

The experiments by Williamson and Nealey [19] also reported a reduced tendency for thin-film blends to macrophase separate. They examined diblock copolymer blends from $\alpha = 0.34$ for which there is no macrophase separation to $\alpha = 0.11$ where macrophase separation readily occurs. In their case, the surfaces were sufficiently neutral that both large and small lamellae oriented perpendicularly to the film. Naturally, the macrophase separation occurred in the lateral direction given the perpendicular orientation of the lamellae. Even still, the domains of the two phases remained very small, emphasizing again just how slow any long-range exchange of material is. As a result of the small domains, the films still contained an extensive amount of boundary between the coexisting phases, which suppressed macrophase separation just as for our system.

As mentioned earlier, the surface affinities of the two walls do not have to be explicitly included in the SCFT calculation when the centers of the lamellae are sufficiently pure, which conveniently reduces the number of relevant system parameters by two. This is because a surface affinity does not affect morphologies that already exhibit a pure concentration at the wall; all it does is increase their free energies by a fixed amount equal to the surface tension of the preferred component times the area of the wall. However, the surface affinities must be included as soon as the domain centers contain a significant fraction of the unfavorable component, because they enhance the segregation at the walls. This decreases the entropy, and consequently the surface tension of the short-period lamellar phase will then become greater than that of the long-period lamellar phase. Thus the short-period lamellar phase will in general favor the wall with the weaker affinity. If the tension of the short-period phase becomes too great, it may become advantageous to have the long-period phase wet both walls with the short-period phase in the middle of the film.

Note that the two experiments [18, 19] on thin film blends actually correspond to soft confinement, where the

[2] The A/B interfacial tension for the parameters of our blend is $\gamma_{\mathrm{A/B}} \approx k_BTa\rho_0(\chi/6)^{1/2} = 5.77k_BTa\rho_0N_\ell^{-1/2}$.

top of the film is in contact with air as opposed to a hard wall. This permits terrace formation, where the film can further reduce its free energy by separating into coexisting thicknesses [6, 38–41]. Although this did not happen in these particular experiments probably because they involved perpendicular lamellae, we would expect it to occur for the soft confinement of parallel lamellae. In principle, the coexisting terraces would be determined by applying a double-tangent construction to the free energy curves for films of uniform thickness [36]. However, the flow of material to the higher terrace could lead to lateral variations in the composition of the blend. Even if the variations were small to start with, the broken homogeneity of the film would facilitate an exchange of large and small molecules between the two film heights. The free energy minimization would have to take this into account. It is also very possible that the system would never reach the true equilibrium, in which case one might have to resort to dynamical simulation in order to predict the behavior. Furthermore, it would have to be a remarkably accurate simulation capable of capturing the subtle physics responsible for the macrophase separation of large and small block copolymers.

5 Summary

This study was motivated by the fact that blending large and small block copolymers is a simple way of controlling the preferred domain size of microstructures used in applications involving confinement. The concern, however, is that confinement may seriously reduce the miscibility of the blend. To address this issue, we selected a simple model system, symmetric AB diblock copolymers confined between two flat walls separated by a distance L. The diblock copolymers were chosen to be well segregated ($\chi N_\ell = 200$ and $\chi N_s = 20$) with a sufficient size difference ($\alpha \equiv N_s/N_\ell = 0.1$) to cause bulk melts to macrophase separate into large and small lamellae for blend compositions of $0.2836 < \bar{\phi}_s < 0.9895$. Our focus was on walls with an affinity for A-type segments (*i.e.*, symmetric wetting), where the melt forms an even number ν of monolayers parallel to the film. As suggested by recent experiments [18], we assumed that any macrophase separation in the film would be limited to the normal direction (see fig. 1b), for which no long-range transport of material is required.

The effect of confinement on the miscibility of the blend was determined from phase diagrams (see fig. 7) constructed by comparing the free energies of mixed M_ν and macrophase-separated S_ν morphologies (see fig. 1), using self-consistent field theory (SCFT). To enhance our understanding, we devised a semi-analytical approximation that illustrates the complex interplay of issues involved in selecting the number of large and small monolayers, $\nu^{(\ell)}$ and $\nu^{(s)}$, in the formation of S_ν morphologies with $\nu = \nu^{(\ell)} + \nu^{(s)}$. The semi-analytical calculation predicts phase boundaries in excellent agreement with the full calculation, and furthermore it is computationally less intensive and more stable, particularly for thicker films. The only significant difference is that the semi-analytical calculation predicts phase transitions as a monolayer switches between large and small (*i.e.*, $\nu^{(\ell)} \to \nu^{(\ell)} \pm 1$ and $\nu^{(s)} \to \nu^{(s)} \mp 1$), whereas the full SCFT predicts an abrupt but nevertheless continuous transformation (see fig. 5).

Although the complicated constraints of confinement can either enhance or suppress macrophase separation, the effects are relatively small. The bigger effect, particularly for small L, comes from the unfavorable boundary tension, Γ_b, between the large and small lamellae, which causes an overall suppression of macrophase separation. This is consistent with experiments [19] that observed a reduced two-phase region in thin films, which we similarly attribute to an extensive boundary between the coexisting phases. This enhanced miscibility will be good news for those wishing to use blending as a way of controlling the properties of a block copolymer melt (*e.g.*, its preferred domain size). Hopefully, our SCFT calculations will also motivate future experiments on the model system considered in this study. Not only is it a good way of exploring the intriguing tendency for large and small block copolymers to macrophase separate, it could also provide a means of measuring the boundary tension between the coexisting phases.

This work was supported by start-up funds from the University of Waterloo, and calculations were performed on the Shared Hierarchical Academic Research Computing Network (SHARCNET) of Compute Canada.

References

1. M.S. Turner, Phys. Rev. Lett. **69**, 1788 (1992).
2. P. Lambooy, T.P. Russell, G.J. Kellogg, A.M. Mayes, P.D. Gallagher, S.K. Satija, Phys. Rev. Lett. **72**, 2899 (1994).
3. N. Koneripalli, N. Singh, R. Levicky, F.S. Bates, P.D. Gallagher, S.K. Satija, Macromolecules **28**, 2897 (1995).
4. N. Koneripalli, R. Levicky, F.S. Bates, M.W. Matsen, S.K. Satija, J. Ankner, H. Kaiser, Macromolecules **31**, 3498 (1998).
5. G.E. Stein, E.W. Cochran, K. Katsov, G.H. Fredrickson, E.J. Kramer, X. Li, J. Wang, Phys. Rev. Lett. **98**, 158302 (2007).
6. A.B. Croll, M.W. Matsen, A.C. Shi, K. Dalnoki-Veress, Eur. Phys. J. E **27**, 407 (2008).
7. V. Mishra, S. Hur, E.W. Cochran, G.E. Stein, G.H. Fredrickson, E.J. Kramer, Macromolecules **43**, 1942 (2010).
8. M. Ilton, P. Stasiak, M.W. Matsen, K. Dalnoki-Veress, Phys. Rev. Lett. **112**, 068303 (2014).
9. M.W. Matsen, Curr. Opin. Colloid Interface Sci. **3**, 40 (1998).
10. M.J. Fasolka, A.M. Mayes, Annu. Rev. Mater. Res. **31**, 323 (2001).
11. C. Park, J. Yoon, E.L. Thomas, Polymer **44**, 6725 (2003).
12. I.W. Hamley, Nanotechnology **14**, R39 (2003).
13. S.B. Darling, Prog. Polym. Sci. **32**, 1152 (2007).
14. I.W. Hamley, Prog. Polym. Sci. **34**, 1161 (2009).
15. H.C. Kim, S.-M. Park, W.D. Hinsberg, Chem. Rev. **110**, 146 (2010).

16. A.-C. Shi, B. Li, Soft Matter **9**, 1398 (2013).
17. H. Yabu, T. Higuchi, H. Jinnai, Soft Matter **10**, 2919 (2014).
18. J. Zhang, D. Posselt, D.-M. Smilgies, J. Perlich, K. Kyriakos, S. Jaksch, C.M. Papdakis, Macromol. Rapid Commun. **35**, 1622 (2014).
19. L.D. Williamson, P.F. Nealey, Macromolecules **48**, 3997 (2015).
20. R. Yang, B. Li, Langmuir **28**, 1569 (2012).
21. K.G. Yager, E. Lai, C.T. Black, ACS Nano **8**, 10582 (2014).
22. Z. Wang, J. Shao, H. Pan, X. Feng, P. Chen, R. Xia, X. Wu, J. Qian, Chem. Phys. Chem. **16**, 567 (2015).
23. J. Song, Y. Li, Q. Huang, T. Shi, L. An, J. Chem. Phys. **127**, 094903 (2007).
24. J.-X. Pan, J.-J. Zhang, B.-F. Wang, H.-S. Wu, M.-N. Sun, Chin. Phys. B **22**, 026401 (2013).
25. L.-C. Zhang, M.-N. Sun, J.-X. Pan, B.-F. Wang, J.-J. Zhang, H.-S. Wu, Chin. Phys. B **22**, 096401 (2013).
26. S.-B. Park, W.-C. Zin, J. Polym. Sci. Part B **51**, 1393 (2013).
27. J. Rao, H. Ma, J. Baettig, S. Woo, M.C. Stuparu, J. Bang, A. Khan, Soft Matter **10**, 5755 (2014).
28. J. Xu, K. Wang, Y. Yang, H. Zhou, X. Xie, J. Zhu, Langmuir **31**, 12354 (2015).
29. M.W. Matsen, F.S. Bates, Macromolecules **28**, 7298 (1995).
30. T. Hashimoto, K. Yamasaki, S. Koizumi, H. Hasegawa, Macromolecules **26**, 2895 (1993).
31. T. Hashimoto, S. Koizumi, H. Hasegawa, Macromolecules **27**, 1562 (1994).
32. M.W. Matsen, J. Chem. Phys. **103**, 3268 (1995).
33. A. Ranjan, J. Qin, D.C. Morse, Macromolecules **41**, 942 (2008).
34. P. Stasiak, M.W. Matsen, Eur. Phys. J. E **34**, 110 (2011).
35. M.W. Matsen, in *Soft Matter, Volume 1: Polymer Melts and Mixtures*, edited by G. Gompper, M. Schick (Wiley-VCH, Weinheim, Germany, 2006).
36. M.W. Matsen, J. Chem. Phys. **106**, 7781 (1997).
37. R. Spencer, M.W. Matsen, Macromolecules **48**, 2848 (2015).
38. G. Coulon, B. Collin, D. Ausserre, D. Chatenay, T.P. Russell, J. Phys. (Paris) **51**, 2801 (1990).
39. B. Collin, D. Chatenay, G. Coulon, D. Ausserre, Y. Gallot, Macromolecules **25**, 1621 (1992).
40. G. Coulon, B. Collin, D. Chatenay, Y. Gallot, J. Phys. II **3**, 697 (1993).
41. P. Stasiak, J.D. McGraw, K. Dalnoki-Veress, M.W. Matsen, Macromolecules **45**, 9531 (2012).